**Proceedings of ASME Turbo Expo 2011**
**GT2011**
**June 6-10, 2011, Vancouver, British Columbia, Canada**

**GT2011-46352**

# ACCURATE CALCULATION OF THE SLIP FACTOR OF AXIAL CASCADES AND IMPELLERS FOR ARBITRARY BLADE SHAPES

**Henrik Smith, Matthias Semel, Philipp Epple, Mihai Miclea-Bleiziffer and Antonio Delgado**
Institute of Fluid Mechanics, LSTM
Friedrich-Alexander University, Erlangen-Nuremberg
Cauerstraße 4, 91058 Erlangen, Germany
Tel: + 49 9131 85-29486, Fax: + 49 9131 85-29503
Corresponding author: henrik.smith@lstm.uni-erlangen.de

## ABSTRACT

*Nowadays, design, redraft and optimisation strategies of axial fans often still rely on the one dimensional mean line theory. However, as it is well known, it is based on a number of assumptions that do not apply to real flow behaviour so that various deviations can be observed. In the present paper, the plane potential theory is used to examine and calculate these deviations. The behaviour of axial cascades is analysed in general and a slip factor is computed. On this basis a quasi-3D calculation method is developed. It is applied to an exemplary impeller and the results are compared with 3D CFD computations. The main characteristic figures are presented and different angle correction and angle exaggeration methods are investigated and compared. Finally, the applicability of the presented method to a precise axial fan design process is illustrated.*

## INTRODUCTION

To estimate the deviations between the one dimensional mean line theory and real flow behaviour, a slip factor can be calculated. The general idea behind this parameter is well known in the literature, e.g. Bohl and Elmendorf [1], Pfleiderer and Petermann [2], Dixon and Hall [3], Lakshminarayana [4]. For radial fans a number of formulae have been developed and examined to estimate the slip factor, e.g. Pfleiderer and Petermann [2], Eck [5]. An overview can be found in Hetzer [6]. Although similar deviations occur in axial fans as well, the procedure is less common for this group of turbomachinery. Pfleiderer and Petermann [2] are among the few that give a formula and lately Qiu et al. [7] presented a slip factor model that shall apply for radial, mixed flow and axial turbomachinery. Apart from that designers rely on deviation angles. Here, intensive studies were performed by Lieblein [8] in the 1950s using NACA 65 profile cascades. A number of improvements have been suggested since then, e.g. by Brodersen [9] and Schiller [10].

Most of the methods have been developed on the basis of measurements, i.e. empirical data, and make use of a specific selection of parameters to calculate the slip factor. Due to the huge number of parameters available for the design of fans, it is rather complicated to exactly capture the flow behaviour inside of the impeller. To overcome these limitations, a method was developed by Hetzer [6] to calculate the exact solution of the plane flow and slip factor in arbitrary radial blade channels. In the current paper a similar method is presented for axial fans. It permits the exact calculation of the slip factor for arbitrary blade shapes. Furthermore it is outlined how this method can be integrated into a high precision design process.

The advantage of the presented method is that it can be applied to arbitrary profiles. Deviation angles as well as slip factors can be calculated without the need of extensive empirical data from measurements. Furthermore a general analysis of cascade behaviour is possible on the basis of the calculated results and will be presented in the current paper. Here, the slip factor is most suitable because it allows the dimensionless characterisation of the deviations between flow angles and blade angles. The analysis can be found in full detail in Smith [11].

 

## 1D MEAN LINE THEORY

One dimensional mean line theory assumes zero blade thickness, ideal fluid flow, an infinite number of blades and thus blade congruent flow. In reality the finite number of blades and their specified thicknesses lead to noticeable deviations between flow angles and blade angles so that the design target will not be reached without further intervention. Furthermore, friction within the fluid and in boundary layers as well as tip gaps will have a considerable influence but are not modeled by the one dimensional theory.

## SLIP FACTOR

To cope with the fact that the flow angles differ from the blade angles, a slip factor is often calculated (e.g. Bohl and Elmendorf [1]). Its purpose is to estimate the drop of total pressure increase and therefore it is defined as the ratio between the accomplished total pressure increase $\Delta p_t$ and the theoretical total pressure increase $\Delta p_{t\infty}$ that is predicted by the one dimensional theory (most often this will be the design goal):

$$\mu = \frac{\Delta p_t}{\Delta p_{t\infty}} \quad . \tag{1}$$

It is important to keep in mind that the slip factor is not a measure for actual losses – it does only model the deviations between the design goal and the achieved total pressure increase due to altered flow angles.

Attempts have been made to estimate this slip factor using basic fan parameters. However, in contrast to radial fans the calculation of this factor for axial fans is rather complicated as it can change significantly with the radius and therefore is dependent on a larger variety of parameters. When dealing with a specific axial fan, the slip factor can be evaluated locally as a function of the radius analoguosly to eq. (1):

$$\mu(r) = \frac{\Delta p_t(r)}{\Delta p_{t\infty}(r)} \quad . \tag{2}$$

However, for a general analysis of axial cascade behaviour this is impractical. It is then more convenient to calculate the slip factor from parameters that are available for any cascade section independently of a specific design (see fig. 1). Using the Euler equation of turbomachinery (e.g. Bohl and Elmendorf [1]), eq. (2) can be rewritten as

$$\mu(r) = \frac{\rho \cdot u(r) \cdot c_{2u}(r)}{\rho \cdot u(r) \cdot c_{2u\infty}(r)} = \frac{c_{2u}(r)}{c_{2u\infty}(r)} = \frac{w_{1u}(r) - w_{2u}(r)}{w_{1u\infty}(r) - w_{2u\infty}(r)} \tag{3}$$

using quantities of the relative system only.

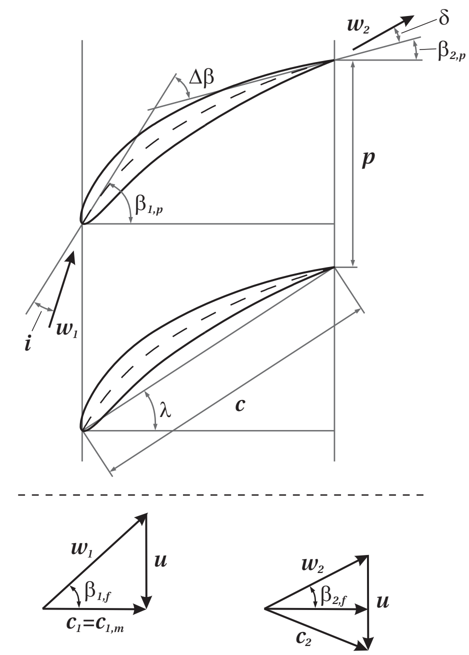


**FIGURE 1**. BASIC PARAMETERS IN AXIAL CASCADES AND VELOCITY TRIANGLES

Pfleiderer [2] suggests the following formula, that is dependent on the blade number $z$, the radius $r$, the axial component of the blade length $e$ and the outlet flow angle $\overline{\beta_2}$ at the radius of the mean flow line $\overline{r}$ (see fig. 2)

$$\mu = \frac{1}{1 + \frac{\chi\left(1+\overline{\beta_2}/60^\circ\right) r}{z \cdot e}} \tag{4}$$

where $\chi$, however, is a coefficient that has to be chosen by experience in the range of $1.0 \ldots 1.2$ and and the radius of the mean flow line $\overline{r}$ is defined as

$$\overline{r} = \sqrt{\frac{r_i^2 + r_a^2}{2}} \quad . \tag{5}$$

There are only few limitations concerning the range of applicability of the modelling of the slip factor. Basically, a slip factor can be calculated for cascades at any pitch to chord ratio $p/c$[1], stagger angle $\lambda$ and incidence angle $i$. Only if adjacent profiles come too close, forcing the flow to accelerate towards higher

[1]The pitch-chord ratio p/c is also known as space-chord ratio. In American practice the inverse pitch-chord ratio, the so-called *solidity* $\sigma = c/p$ is frequently used, e.g. Dixon and Hall [3].

velocities, the solution will become inaccurate as the calculation method is not capable of coping with compressible flow. According to Kümmel [12] gases can be considered as incompressible as long as the Mach number does not exceed a limit of $Ma = 0.3$. For static air at $T = 25^\circ$ and isentropic changes, i.e. $\kappa = 1.4$, this corresponds to a velocity of approximately 100 m/s. A specific pitch to chord ratio limit cannot generally be given as this problem is highly dependent on the actual blade geometry and stagger angle as well as the velocity of the oncoming flow. For increasing $p/c$ ratios the solution converges to the isolated airfoil case. Common fan applications make use of cascade sections in the range of $p/c = 0.5\ldots2.5$ (e.g. Lieblein [8]). Ratios up to 4 may occur at the blade tips of fans with only few blades.

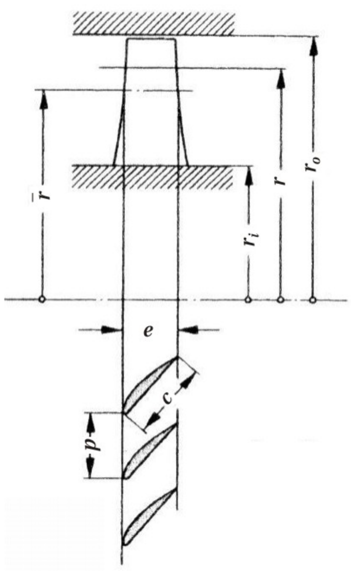


**FIGURE 2**. AXIAL CASCADE (ADOPTED FROM BOHL [13])

## BLADE PROFILES

In the present paper NACA 4 digit airfoil profiles are used for the analysis of cascade behaviour (e.g. Riegels [14]). However, the calculation method presented in the following section is capable of dealing with arbitrary blade shapes, such as other NACA series profiles, Eppler, Göttinger or Kármán-Trefftz airfoils (e.g. Paraschivoiu [15]) as well as individually designed shapes. The three parameters necessary for the complete definition of such a profile are the maximum camber $f$, the position of maximum camber $g$ and the thickness $t$. While the last parameter can be given independently, the first two have to be calculated inversely depending on the desired inlet and outlet blade angles. According to Lakshminarayana [4] the blade turning angle is defined as

$$\Delta\beta = \beta_{1,p} - \beta_{2,p} \quad . \tag{6}$$

It is segmented into $\gamma_1$ and $\gamma_2$ (see fig. 3) by means of a balancing factor $b$ that has to be chosen in the range $0 < b < 1$:

$$\gamma_1 = b \cdot \Delta\beta \tag{7}$$
$$\gamma_2 = (1-b) \cdot \Delta\beta \quad . \tag{8}$$

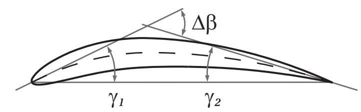


**FIGURE 3**. PARAMETERS FOR THE INVERSE DEFINITION OF A NACA 4 DIGIT PROFILE

This is sufficient to solve for $f$ and $g$ using a set of two linear equations. Adequate camber lines were found to be generated with a balancing factor of $b = 0.6$. This is a good compromise between ensuring high slip factors and minimising the local curvature of the profile and therefore the tendency of boundary layer separation. With $b$ set, $\gamma_1$ and consequently the stagger angle $\lambda$ can be calculated as:

$$\lambda = \beta_{1,p} - \gamma_1 \quad . \tag{9}$$

## 2D PLANE POTENTIAL FLOW

### Basic assumptions

The three basic equations of the potential theory are the continuity equation, Bernoulli's equation and the irrotationality condition. This implies frictionless and incompressible fluids. Potential flows can be modeled in the second and third dimension. The present paper concentrates on the plane potential flow as this leads to fairly accurate results. The flow is calculated on coaxial sections of the impeller, thus modelling the flow through a cascade of blade profiles.

### Cascade flow

To calculate the plane potential flow a *vortex panel method* was implemented based on the method of Lewis [16]. The blade profile is discretised into linear panels and covered with vorticity sheets of initially unknown strengths. The velocity that is induced by the whole set of vorticity sheets superimposed with the oncoming parallel flow has to be zero perpendicular to each of the panels, i.e. on the profile surface. Additionally the Kutta condition (e.g. Katz and Plotkin [17]) has to be fulfilled at the trailing edge. This leads to a system of linear equations that can be solved numerically to yield the vorticity strengths and consequently the velocities on the profile surface. The method was originally developed by Martensen [18] and therefore is often referred to as the *Martensen method*. Basically this is a common procedure for isolated airfoils and it has to be modified in order to model the influence of the cascade. This is done by first deriving the velocities that are induced by the vorticity sheets of the examined profile itself and its adjacent profiles. The result is an infinite series that can be collapsed back into a single term. Thus an "infinite" cascade can be modeled with the same computational effort as a single airfoil. The obtained solution is identical for each of the profiles and periodical concerning the flow field within the blade channel. The numerical modelling process is described in detail in Lewis [16]. For the present paper, a discretisation of 1000 panels is chosen for the profile and the panel density is increased at the leading and trailing edges. This was found to be the best compromise between accuracy and calculation speed. A very good convergence of the crucial parameters, such as the lift coefficient and the slip factor can be observed at this point.

## 2D CFD SIMULATION SETUP

2D CFD simulations were performed with ANSYS CFX®12.1. To achieve a fully two-dimensional flow of a cascade section, only one mesh cell was simulated in the third dimension and a symmetry boundary condition was set at the corresponding surfaces (see fig. 4). As inlet boundary condition a velocity was given together with the angle of the oncoming flow and a static ambient temperature of $T_a = 25\,^{\circ}\mathrm{C}$. At the outlet a static ambient pressure of $p_a = 101\,325$ Pa is set. The reference density is $\rho_a = 1.184\,\mathrm{kg/m^3}$. A translational periodicity interface is used at the upper and lower boundary surface. Thus only one profile is necessary to model the behaviour of the cascade.

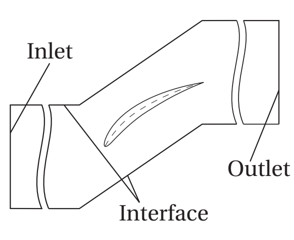


**FIGURE 4**. 2D CFD SIMULATION SETUP

Two variants were simulated to show the transition from a frictionless quasi-3D flow to a viscous flow involving wall friction: One with wall friction disabled at the blade using the *free slip* boundary condition and one with wall friction enabled using the *no slip* boundary condition. All CFD simulations are performed using the *Shear Stress Transport* turbulence model (e.g. Menter [19]) which is industry standard today. A fully developed turbulent flow was assumed at the inlet (zero gradient option).

A block-structured hexahedral grid is used including a C-mesh (e.g. Cebeci et al. [20]) around the airfoil and an increased mesh density in the near-wall region. A grid study was performed to ensure the independency of the solution from the number of nodes. For pitch to chord ratios of $p/c = 1$ independency was achieved for approx. 110 000 nodes.

## ANALYSIS OF CASCADE BEHAVIOUR

In the current and all following sections the leading edge blade angle $\beta_{1,p}$ is set identical to the angle of the oncoming flow $\beta_{1,f}$ to ensure shockless inflow. This implies zero incidence angles $i = 0°$, i.e. $\beta_1 = \beta_{1,f} = \beta_{1,p}$.

The solution of the plane potential flow is independent of the velocity of the oncoming flow concerning outlet flow angle deviations. The same accounts for the slip factor that can be calculated as a ratio of velocity differences (see eq. (3)).

In the following sections, the influence of the inlet flow angle $\beta_1$, the blade turning angle $\Delta\beta$ and the blade thickness $t$ on general cascade behaviour is investigated and discussed.

### Influence of the inlet flow angle

If the blade turning angle $\Delta\beta$ is kept constant while altering $\beta_1$, it can be observed based on the vortex panel code implemented that for an increasing inlet flow angle the slip factor decreases (see fig. 5). It is remarkable that in a small range around $p/c = 1.1$ all curves show a particular behaviour. For $\beta_1 = 75°$ an explicit slip factor maximum arises. With inlet flow angles decreasing this maximum becomes less apparent and finally vanishes ($\beta_1 = 45°$). On the right hand side of this section around $p/c = 1.1$ the slip factor decreases for increasing pitch to chord ratios. On the left hand side the behaviour is vice versa for large inlet flow angles ($\beta_1 = 75°$). Only around $p/c = 0.5$ a slight increase can be observed for decreasing values of $\beta_1$ finally resulting in a curve that is characterised by negative slope only ($\beta_1 = 45°$). Referring to the corresponding outlet flow deviation angles $\delta$ (see fig. 6) minima can be observed at the very same pitch to chord ratios where the slip factor maxima are located. This is to be expected since the outlet flow angle $\beta_{2,f}$ is directly linked to the relative circumferential velocity $w_{2u}$.

### Influence of the blade turning angle

The appearance of a slip factor maximum is also linked to the blade turning angle $\Delta\beta$ (see fig. 7). For higher values of

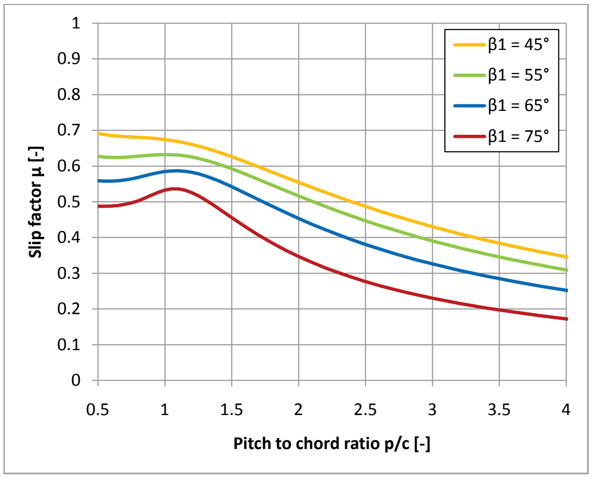


**FIGURE 5**. IMPACT OF DIFFERENT INLET FLOW ANGLES ON THE SLIP FACTOR ($\Delta\beta = 10°$, $t = 10\,\%$)

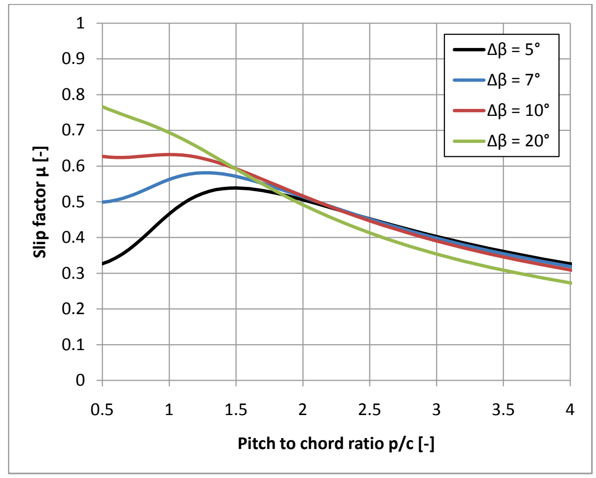


**FIGURE 7**. IMPACT OF THE BLADE TURNING ANGLE ON THE SLIP FACTOR ($\beta_1 = 55°$, $t = 10\,\%$)

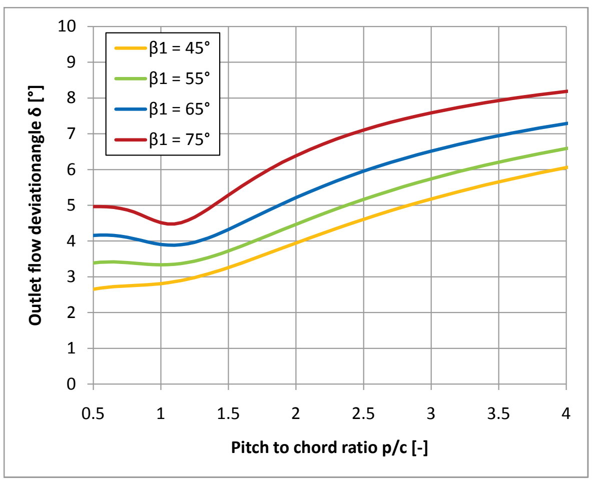


**FIGURE 6**. IMPACT OF DIFFERENT INLET FLOW ANGLES ON THE OUTLET FLOW DEVIATION ANGLE ($\Delta\beta = 10°$, $t = 10\,\%$)

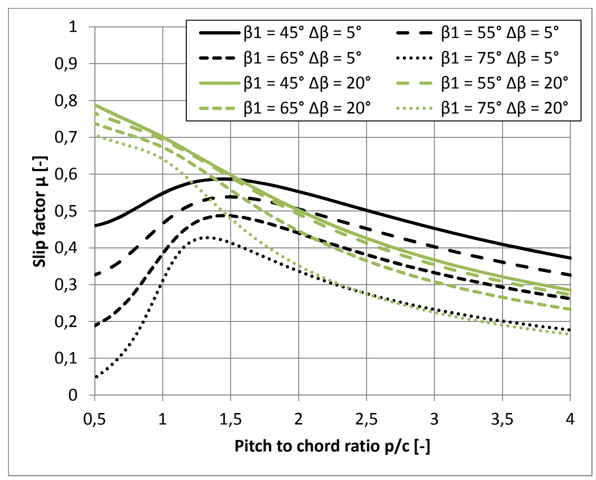


**FIGURE 8**. IMPACT OF THE BLADE TURNING ANGLE AND THE INLET FLOW ANGLE ON THE SLIP FACTOR ($t = 10\,\%$)

$\Delta\beta > 20°$ it does almost vanish, whereas for decreasing values it manifests even more clearly. Apart from that the maximum moves to higher pitch to chord ratios. This indicates a specific $p/c$ value for each different type of cascade section that leads to an optimum slip factor, i.e. a maximum slip factor.

Fig. 8 shows the dependency of the slip factor with respect to the inlet flow angle. The higher $\beta_1$ the lower the slip factor will be. Moreover, the influence of increasing $\beta_1$ values on the slip factor is obviously stronger for smaller blade turning angles $\Delta\beta$. The maximum will also become more evident with higher inlet flow angles. In doing so it moves slightly towards lower pitch to chord ratios. One should remark that the 1D mean line theory does not include any influence of the inlet angle $\beta_1$.

## Influence of the blade thickness

When it comes to blade thickness the differences do seem to be marginal at higher pitch to chord ratios. Below $p/c = 1.5$ the situation is different – here thinner blades result in higher slip factors (see fig. 9). This could be confirmed with 2D CFD computations (figure not shown). The lower the pitch to chord ratio is chosen the bigger the gap gets. Moreover, the slip factor maximum that has been appearing for higher inlet flow angles $\beta_1$ vanishes for decreasing blade thickness. At the same time the impact of the blade turning angle $\Delta\beta$ decreases (see fig. 10). The comparison between fig. 10 and 7 again reveals the tendency of the slip factor being considerably higher for thinner blades at pitch to chord ratios below $p/c = 1.5$.

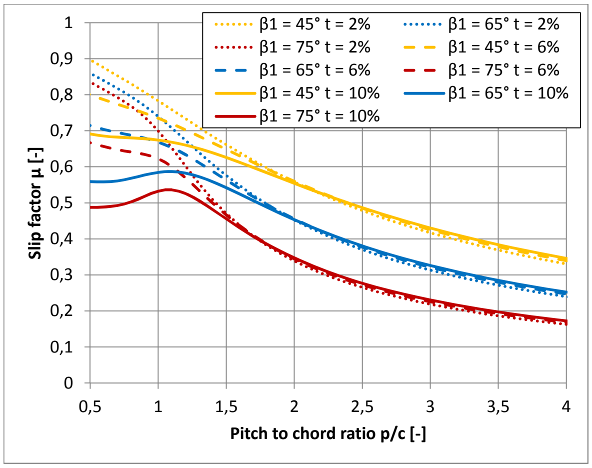


**FIGURE 9**. IMPACT OF THE BLADE THICKNESS ON THE SLIP FACTOR ($\Delta\beta = 10°$)

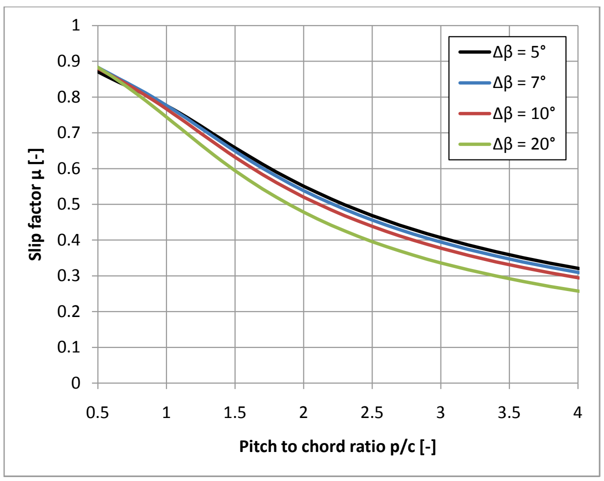


**FIGURE 10**. IMPACT OF THE BLADE TURNING ANGLE ON THE SLIP FACTOR ($\beta_1 = 55°, t = 2\,\%$)

## 2D INTEGRATED/QUASI-3D METHOD

A two dimensional integrated method is used to calculate the flow in the fan in a quasi-three-dimensional way. Therefore, the potential flow is calculated on a number of coaxial sections that are distributed over the radius of the blade. The individual results are then integrated and mass flow averaged. Radial velocities cannot be considered by this model. However, even with flow angles deviating from the actual profile angles at the trailing edge this is unproblematic at the design point and within a moderate range of partial load and overload conditions as it is shown later.

The presented quasi-3D method is used both for the calculation of design and offdesign conditions. Thereby constant meridian velocity is assumed for all cases. The author is aware that this is a simplification. An extension of the one dimensional mean line theory for forced vortex designs at design and offdesign conditions is currently prepared for publication by the authors [21]. It permits the calculation of the meridian velocity as a function of the radius and will be integrated in the current method and presented in a further publication.

The advantages of this method are based on the computational effort that is necessary to calculate the flow in an impeller. Common 3D CFD simulations still need extensive computing power to provide results within short time, even if just one blade channel is computed as it is done here. In contrast, using the 2D integrated method results can be obtained in a small fraction of this time. It is therefore highly feasible to be used in an integrated design and optimisation process.

| Parameter | Variable | Value |
|---|---|---|
| Volumetric flow | $\dot{V}$ | $4\ m^3/s$ |
| Total pressure increase | $\Delta p_t$ | 1500 Pa |
| Specific speed | $\sigma$ | 0.9925 |
| Specific diameter | $\delta$ | 1.4837 |
| Outer diameter | $d_o$ | 472 mm |
| Inner diameter | $d_i$ | 264 mm |
| Hub to tip ratio | $m$ | 0.56 |
| Number of blades | $z$ | 10 |
| Reynolds number | $Re_{blade}$ | 500000 |

**TABLE 1**. DESIGN TARGET VALUES OF THE EXEMPLARY IMPELLER

## CASE STUDY

An exemplary impeller is used to confirm the results of prior sections and to evaluate different angle correction and exaggeration methods. The design parameters can be found in tab. 1. The basic setup is designed assuming constant meridional velocities and angular momentum over the whole radius. Thus, a radial equlibrium between streamlines on coaxial sections should theoretically be achieved according to the one-dimensional mean line theory, i.e. if the angles of the outgoing flow $\beta_{2,f}$ comply with the blade angles $\beta_{2,p}$ given by the design. The leading edge blade angles $\beta_{1,p}$ are chosen identical to the angles of the oncoming flow $\beta_{1,f}$ to ensure shockless inflow. A detailed discussion of this topic can be found in Carolus [22]. The blade number is chosen to 10 based on the quasi-3D results for the slip factor, which is found to be maximal for this setting. For the basic setup (see fig. 11) no angle correction method is applied.

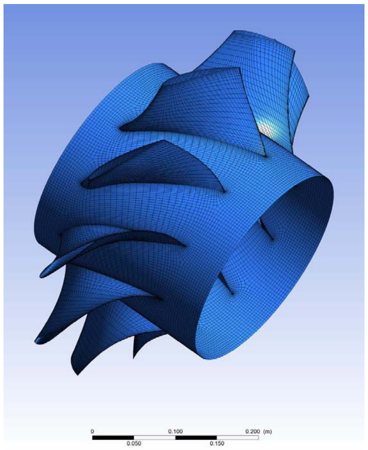

**FIGURE 11**. ROTOR OF THE EXEMPLARY IMPELLER BASIC SETUP

## 3D CFD SIMULATION SETUP

The 3D CFD simulations are performed with ANSYS CFX®12.1. To reduce complexity, the hub and shroud radii are kept constant from inlet to outlet and a tip gap is not modeled. The quasi-3D solution is periodical, i.e. identical for each blade channel. Therefore the 3D CFD simulations are performed in a similar way modelling a single passage using a rotational periodicity interface and a constant pitch of 36° according to the blade number of $z = 10$.

The simulation is composed of three domains – inlet, blade and outlet (see fig. 12). Basic dimensions can be found in tab. 2. They are connected by means of a *Frozen Rotor* interface. The inlet boundary condition is set to a static ambient pressure of $p_a = 101\,325$ Pa and a static temperature of $T_a = 25$ °C. These settings are identically applied to the quasi-3D calculations. A mass flow is given at the outlet according to the specified volumetric flows and a reference density of $\rho_a = 1.184\,\mathrm{kg/m^3}$. The distributions that will be shown in the following sections, e.g. of the velocity before and behind the rotor, will be evaluated on the planes given in fig. 12.

Two variants are simulated to show the transition from a frictionless quasi-3D flow to a viscous flow involving wall friction: One with wall friction disabled at the blade and all walls using the *free slip* boundary condition and one with wall friction enabled using the *no slip* boundary condition. All CFD simulations are performed using the *Shear Stress Transport* turbulence model (e.g. Menter [19]) which is industry standard today. A fully developed turbulent flow was assumed at the inlet (zero gradient option).

A block-structured hexahedral grid is used for all three flow domains including an O-Grid around the blade (see fig. 11). The mesh density is increased in the near-wall regions of the blade, hub and shroud. A grid study was performed to ensure the in-

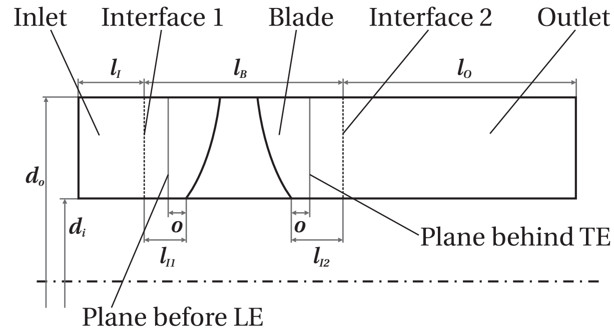


**FIGURE 12**. SIMULATION SETUP

| **Parameter** | **Variable** | **Value** |
|---|---|---|
| Inlet axial length | $l_I$ | 250 mm |
| Blade axial length | $l_B$ | 250 mm |
| Outlet axial length | $l_O$ | 1000 mm |
| Axial offset | $o$ | 30 mm |
| Distance interface/leading edge | $l_{I1}$ | $\approx$ 35 mm |
| Distance trailing edge/interface | $l_{I2}$ | $\approx$ 50 mm |

**TABLE 2**. BASIC DIMENSIONS OF THE SIMULATION SETUP

dependency of the solution from the number of nodes. Independency was achieved for approx. 120 000 nodes per blade channel.

## COMPARISON OF 2D AND 3D COMPUTATIONS

### $C_p$ distributions

Figures 13–17 indicate the potential that lies in the calculation of the plane potential flow of cascade sections. Here, the $C_p$ distribution is shown for several span values s. Apart from small deviations on the pressure side of the profile, the 2D potential flow and 2D CFD computations differ only marginally in the area of the leading edge. While the impact of friction is negligible here it is not in the area of the trailing edge. There the *no slip* boundary condition leads to lower $C_p$ values. This is the result of the developing boundary layer, precisely its displacement thickness. As a result the oncoming mass flow has to accelerate because the flow area is slightly decreasing. The higher velocities then cause lower $C_p$ values. This is supported by the fact that the deviations in the area of the trailing edge do have an increasing extent towards lower span values. Here, the relative velocities the blade is exposed to are lower so that the boundary layer will be of higher thickness (e.g. Schlichting and Gersten [23]).

However, the differences between 2D and 3D calculations are more pronounced. The deviations are apparent mainly at hub and shroud. In between a good resemblance between 2D potential flow, 2D CFD and 3D CFD results can be observed. While at the hub the $C_p$ distribution differs over the whole chord length, the deviations at the shroud affect in particular the leading edge.

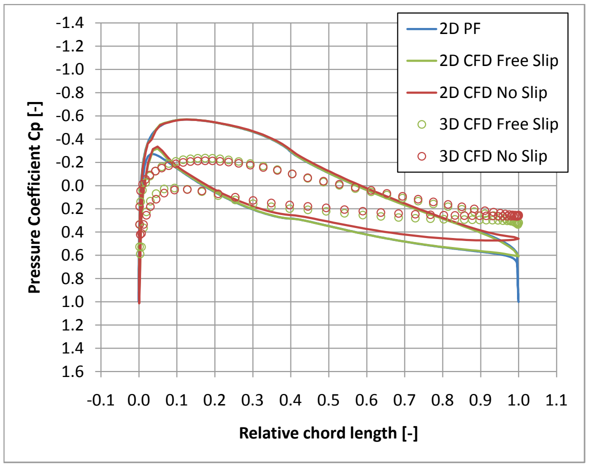


**FIGURE 13**. COMPARISON BETWEEN 2D POTENTIAL FLOW, 2D CFD AND 3D CFD $C_p$ DISTRIBUTIONS FOR $s = 0.000$

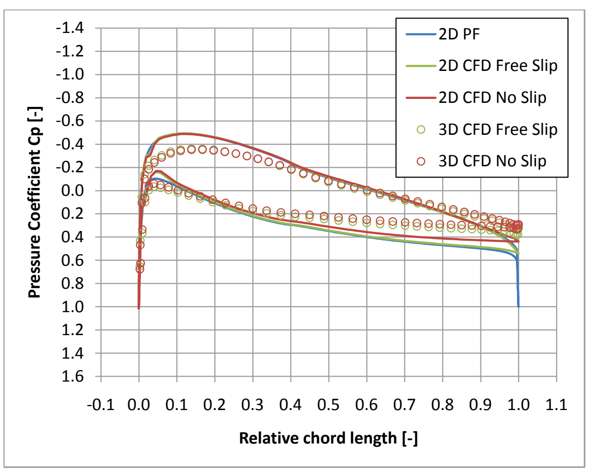


**FIGURE 14**. COMPARISON BETWEEN 2D POTENTIAL FLOW, 2D CFD AND 3D CFD $C_p$ DISTRIBUTIONS FOR $s = 0.266$

### Main characteristic figures

Fig. 18 shows the total and the total to static pressure increase of the exemplary impeller without angle correction methods applied. As expected the deviations between the 1D and

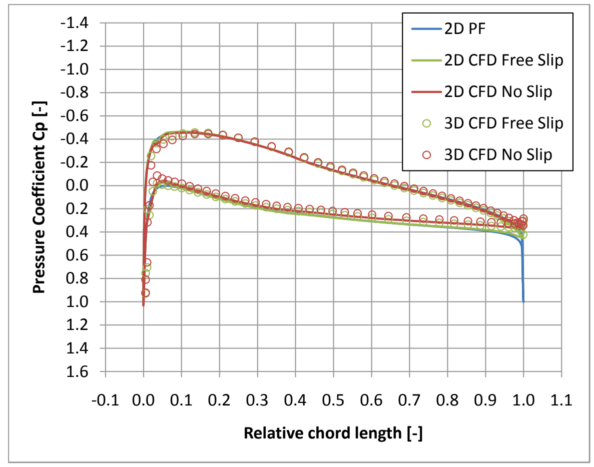


**FIGURE 15**. COMPARISON BETWEEN 2D POTENTIAL FLOW, 2D CFD AND 3D CFD $C_p$ DISTRIBUTIONS FOR $s = 0.544$

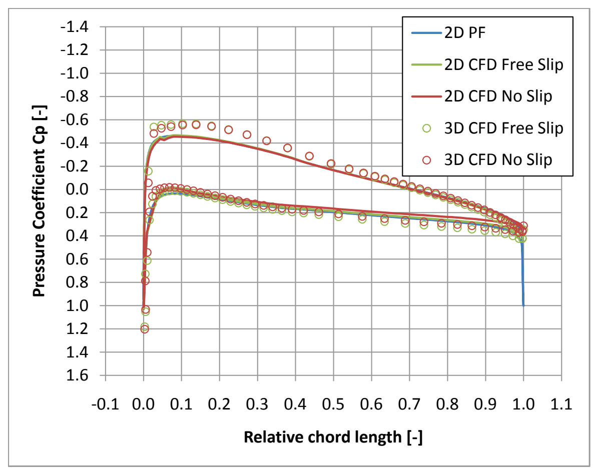


**FIGURE 16**. COMPARISON BETWEEN 2D POTENTIAL FLOW, 2D CFD AND 3D CFD $C_p$ DISTRIBUTIONS FOR $s = 0.785$

3D/quasi 3D predictions are significant. However, the quasi 3D prediction nearly hits the 3D CFD one that has been performed without wall friction. The deviations between the $\Delta p_t$ predictions of the 1D theory and the 3D computations are in the area of 31 % (wall friction disabled) and 41 % (wall friction enabled) whereas the deviations between quasi 3D and 3D results are in the area of 6 % and 20 %. A similar situation can be observed with respect to the total to static efficiency (see fig. 19). In contrast to the 1D mean line prediction the shape of the quasi-3D curve is identical to the one given by the 3D CFD results. The offset between the curves is due to the flow losses.

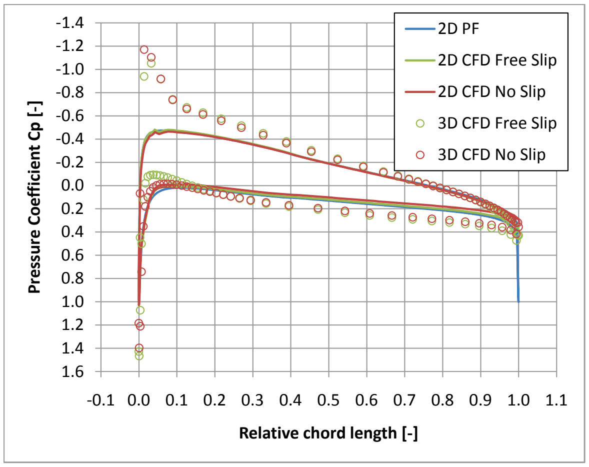


**FIGURE 17**. COMPARISON BETWEEN 2D POTENTIAL FLOW, 2D CFD AND 3D CFD $C_p$ DISTRIBUTIONS FOR $s = 1.000$

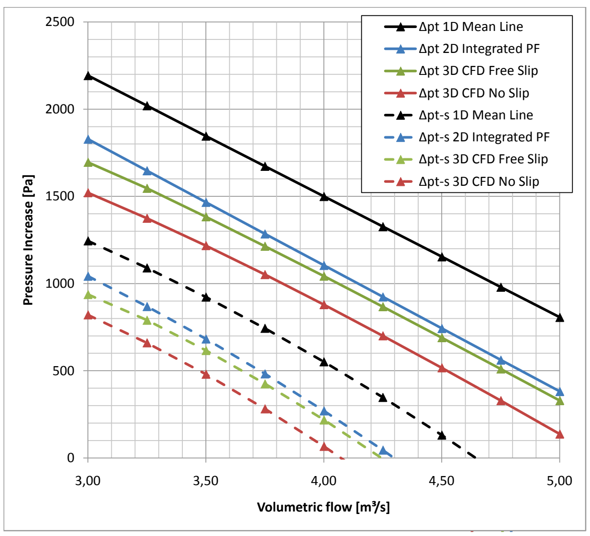


**FIGURE 18**. TOTAL AND TOTAL TO STATIC PRESSURE INCREASE OF THE EXEMPLARY IMPELLER WITHOUT BLADE ANGLE CORRECTION

## Slip factor

Fig. 20 shows the slip factor as a function of the relative blade height. The deviation between blade and flow angles is small at the hub and increases towards the shroud. It is remarkable that both the prediction of Pfleiderer and the quasi-3D prediction have nearly the same shape although the correlation given by Pfleiderer is based on empirical data. It does give a more pronounced prediction than the one that was calculated on the basis of potential flow. In the area of the shroud both the CFD calculation with wall friction disabled and enabled come to lie close to the quasi-3D prediction whereas below span values of about $s = 0.7$ their slip factor lies below. Within this range the *free slip*

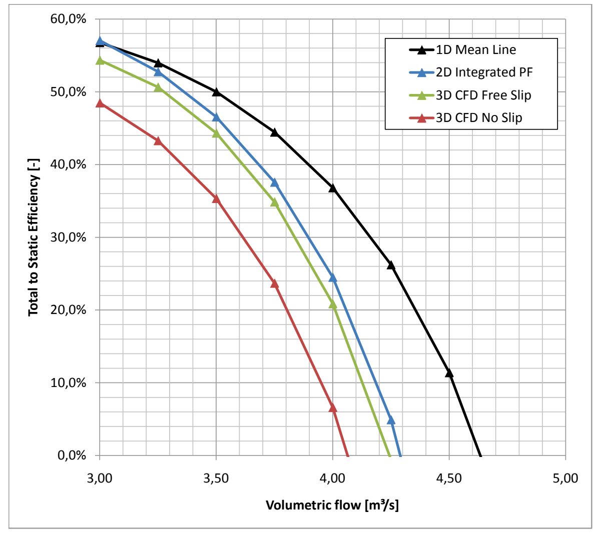


**FIGURE 19**. TOTAL TO STATIC EFFICIENCY OF THE EXEMPLARY IMPELLER WITHOUT BLADE ANGLE CORRECTION

CFD results are in good agreement with the Pfleiderer prediction. The *no slip* calculations do even lie below except in the area of the hub.

However, the calculation of the slip factor from CFD results is not unproblematic as it is based on the comparison of circumferential velocities of one-dimensional theory and three-dimensional computations. While 1D theory assumes constant meridional velocity over the whole radius this is not the case for 3D simulations as it can be seen in fig. 21. Without wall friction this assumption is valid at least for the oncoming flow but not necessarily for the outgoing flow. With wall friction enabled the velocities near hub and shroud decrease resulting in increased meridian velocities in between to compensate for the lack of mass flow in the outer regions. Consequently, the velocity triangles are altered and the precision of the slip factor calculation is reduced. It would be easier to calculate the slip factor on the basis of the total pressure increase. However, in this case it would include actual internal flow losses and therefore miss the essence of the slip factor, which is the deviation of the flow angle from the blade angle.

It can be observed that the flow is moving towards the hub as the radial velocities are below zero over the full blade height (figure not shown). This complies with the behaviour of the meridian velocity (see fig. 21). The maximum radial velocities can be found in the range $0.3 \leq s \leq 0.4$. However, they are in the area of $c_r \approx -0.35\,\mathrm{m/s}$ which corresponds to less than 1 % of the meridional velocity at this point. As this is negligibly small, the assumption of vanishing radial velocities is therefore proper. Similar observations can be made within a moderate range of partial load and overload conditions, i.e. between $3\,\mathrm{m^3/s}$ and $5\,\mathrm{m^3/s}$ (figure not shown).

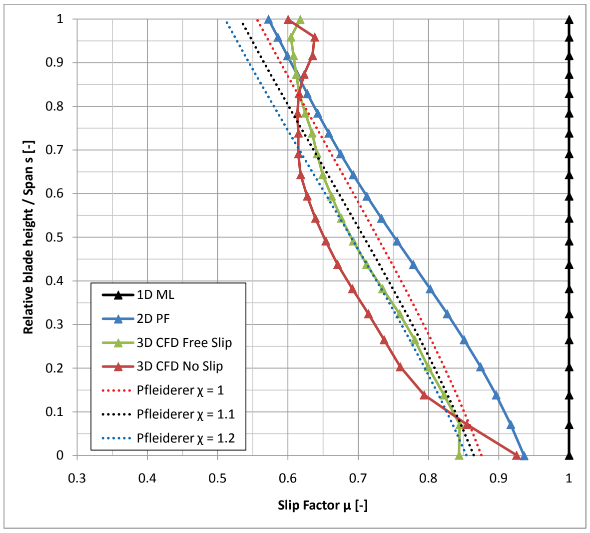


**FIGURE 20**. SLIP FACTOR DISTRIBUTION OF THE EXEMPLARY IMPELLER ($\dot{V} = 4\ \mathrm{m}^3/\mathrm{s}$)

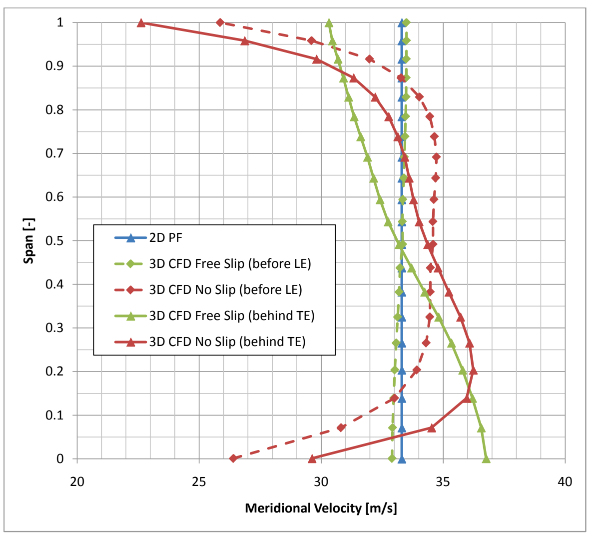


**FIGURE 21**. MERIDIAN VELOCITY DISTRIBUTION OF THE EXEMPLARY IMPELLER ($\dot{V} = 4\ \mathrm{m}^3/\mathrm{s}$)

The analysis of the outlet flow angles $\beta_2$ (fig. 22) reveals only small deviations between the quasi-3D prediction and the 3D CFD results. While the deviation between the flow angles of the *free slip* calculation increases slightly with increasing span values, the deviation of the flow angles of the *no slip* calculation concentrates on the shroud region. Hence, the quasi-3D prediction of the actual flow angles is fairly accurate.

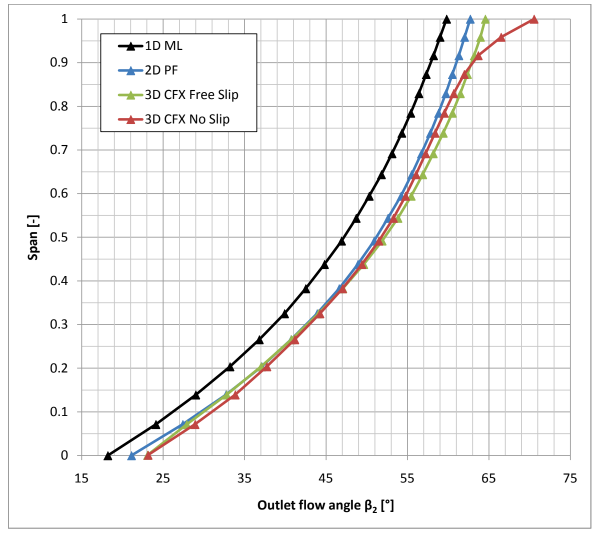


**FIGURE 22**. OUTLET FLOW ANGLE DISTRIBUTION OF THE EXEMPLARY IMPELLER ($\dot{V} = 4\ \mathrm{m}^3/\mathrm{s}$)

### Influence of the blade thickness

In a prior section the slip factor was found to be dependent on the blade thickness. This tendency can be confirmed with respect to three-dimensional impellers as can be seen in tab. 3 and fig. 23. While the Pfleiderer prediction is not able to model the influence of blade thickness, the precision of the quasi-3D method seems to increase with decreasing blade thickness. The general shape of the slip factor distributions is maintained. The curves are tilting slightly rightwards with decreasing blade thickness while the intensity of the the kink of the CFD results in the area of the shroud increases.

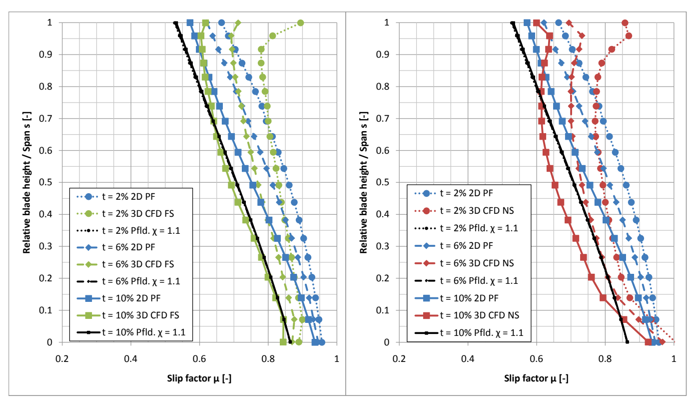


(a) (b)

**FIGURE 23**. SLIP FACTOR DISTRIBUTION OF THE EXEMPLARY IMPELLER – COMPARISON BETWEEN QUASI-3D, PFLEIDERER (a) FREE SLIP 3D CFD AND (b) NO SLIP 3D CFD PREDICTIONS ($\dot{V} = 4\ \mathrm{m}^3/\mathrm{s}$)

| | $\mu_{q3D}$ | $\mu_{3D,FS}$ | $\mu_{3D,NS}$ | $\mu_{Pfl.}$ $(\chi = 1.1)$ |
|---|---|---|---|---|
| $t = 2\,\%$ | 0.829 | 0.832 | 0.817 | 0.686 |
| $t = 6\,\%$ | 0.787 | 0.769 | 0.752 | 0.687 |
| $t = 10\,\%$ | 0.736 | 0.700 | 0.680 | 0.689 |

**TABLE 3**. SLIP FACTOR INTEGRATED VALUES

The total pressure increase at the design point is increasing as well with decreasing blade thickness, as can be seen in fig. 24. For partial load conditions the disadvantages of thinner blades become clearly visible. While the characteristic curve of the impeller with $t = 10\,\%$ is a near to straight line, the one of the impeller with $t = 2\,\%$ cannot achieve this behaviour. This is due to the fact that the leading edge is sharper for thinner blades promoting boundary layer separation for off-design incident flow. At overload conditions no problems can be observed.

Hence, it can be said that thinner blades are clearly beneficial with respect to the slip factor if the fan is not intended to operate within a very broad range aside his operating point. As a consequence of the increased slip factor, a higher total pressure increase $\Delta p_t$ is achieved.

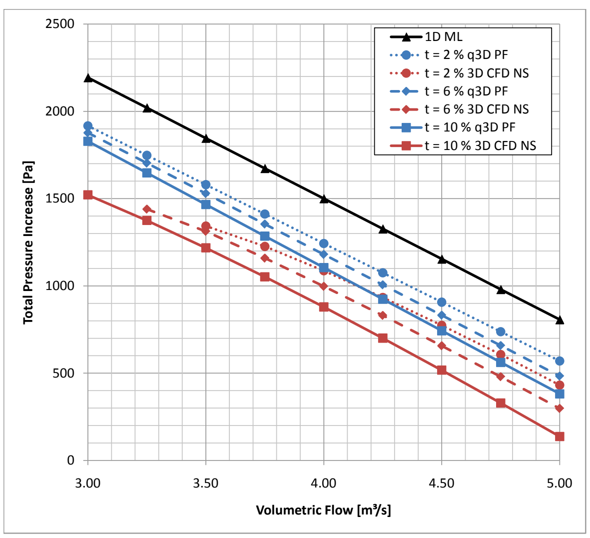


**FIGURE 24**. TOTAL PRESSURE INCREASE CHARACTERISTIC OF THE EXEMPLARY IMPELLER – COMPARISON OF DIFFERENT BLADE THICKNESSES

## ANGLE CORRECTION

As a consequence of the inevitable deviations between blade and flow angles behind the rotor, an angle correction is necessary in order to reach the design goal. Therefore the trailing edge blade angle $\beta_{2,p}$ is modified iteratively on each of the sections calculated by the quasi-3D method until the deviation between the design flow angle and the computed flow angle becomes less than $0.01°$. As for fans the outlet flow deviation angle $\delta$ is always positive (see notation in fig. 1) this implies diminishing the trailing edge profile angle $\beta_{2,p}$. The resultant total pressure increase can be found in fig. 25. As expected, the original design goal of $\Delta p_t = 1500\,\text{Pa}$ is now met with good accuracy at the design point. Furthermore, the quasi-3D characteristic gives a good prediction of the general shape of the 3D CFD characteristic. The same applies for the total to static efficiency $\eta_{ts}$ (see fig. 26). According to Carolus [22] it is defined as

$$\eta_{ts} = \frac{\Delta p_{ts}}{\Delta p_t} = \frac{\Delta p_t - \frac{\rho}{2} c_2^2}{\Delta p_t} \tag{10}$$

The shape of the characteristic is altered due to the blade angle correction and complies now to the originally intended design (black curve). The offset between the quasi-3D, *free slip* 3D CFD and *no slip* 3D CFD predictions is maintained. It is important to keep in mind that the essence of this efficiency is not to give an information solely about hydraulic losses. The total to static efficiency describes the extent to which the total pressure increase that is generated by the fan is transformed into static pressure. In most of the cases the additional dynamic pressure at the exit of the impeller cannot be used and must therefore be considered as an actual loss. The total to static efficiency is therefore a proper performance criterion and is used as such in design methods, e.g. by Epple [24].

The results indicate that the described angle correction method enables the designer to achieve a nearly constant total pressure increase over the full blade height (see fig. 27) by correcting the outlet flow angles $\beta_2$ (see fig. 28). Due to flow losses this is however not sufficient to achieve the design goal of a total pressure increase of $\Delta p_t = 1500\,\text{Pa}$. The use of an angle exaggeration method is therefore an immediate consequence.

## ANGLE EXAGGERATION

To compensate for flow losses and finally achieve the intended design goal, angle exaggeration methods have been developed. A method based on empirical data was developed by Lieblein [8] on the basis of measurements taken on cascades with NACA 65 profiles. A number of improvements have been suggested, e.g. by Brodersen and Schiller – a comparison can be found in Bommes [25]. In the current section, these methods are applied to the exemplary impeller and their applicability is examined.

On the basis of the angle correction method described in the prior section, two exaggeration methods have been developed

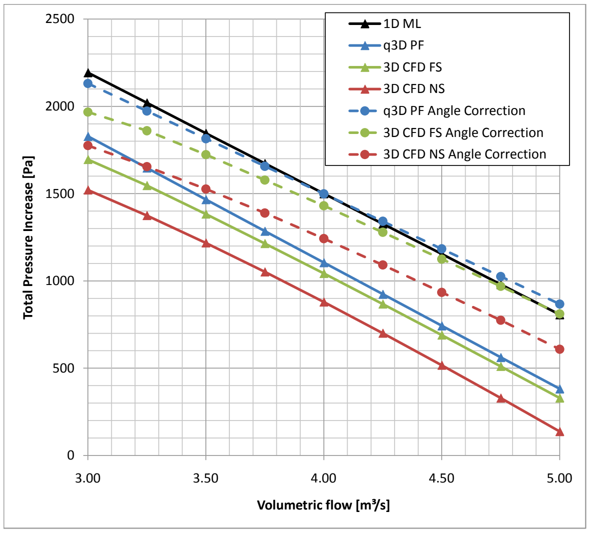


**FIGURE 25**. TOTAL PRESSURE INCREASE CHARACTERISTIC – COMPARISON OF CORRECTED AND UNCORRECTED TRAILING EDGE PROFILE ANGLES

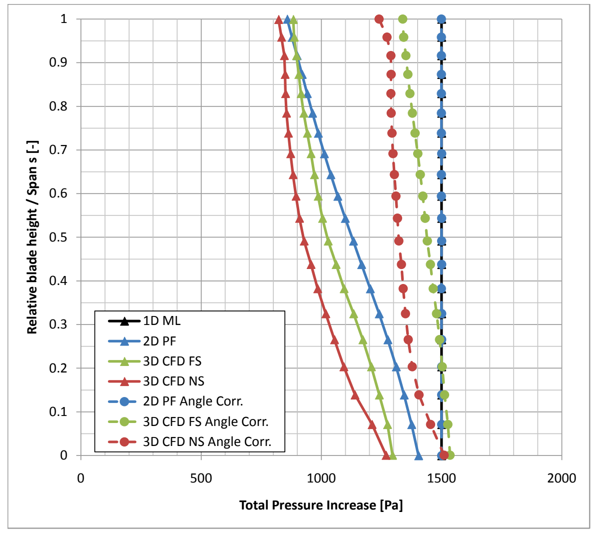


**FIGURE 27**. TOTAL PRESSURE INCREASE DISTRIBUTION – COMPARISON OF CORRECTED AND UNCORRECTED TRAILING EDGE PROFILE ANGLES

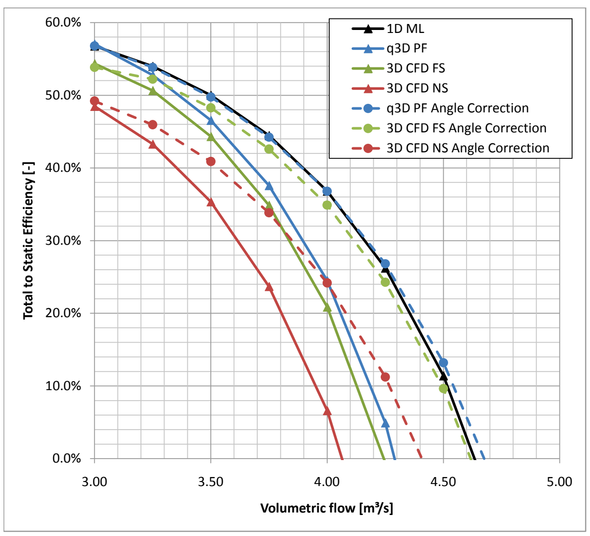


**FIGURE 26**. TOTAL TO STATIC EFFICIENCY CHARACTERISTIC – COMPARISON OF CORRECTED AND UNCORRECTED TRAILING EDGE PROFILE ANGLES

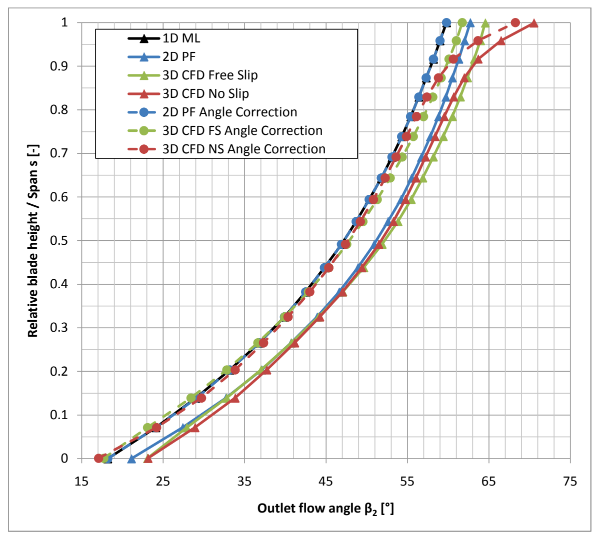


**FIGURE 28**. OUTLET FLOW ANGLE $\beta_2$ DISTRIBUTION – COMPARISON OF CORRECTED AND UNCORRECTED TRAILING EDGE PROFILE ANGLES

and examined by the author. Both methods alter the trailing edge profile angles $\beta_{2,p}$ iteratively until the estipulated flow angles $\beta_{2,f}$ are achieved. The *constant angle exaggeration* method diminishes the design outlet flow angles $\beta_{2ds,f}$ by a constant value $\tau$

$$\beta_{2ex,f} = \beta_{2ds,f} - \tau \tag{11}$$

whereas the *weighted angle exaggeration* method diminishes the design outlet flow angles $\beta_{2ds,f}$ by a value $\tau$ that is a constant fraction $\varepsilon$ of the flow turning angle $\Delta\beta_f$ at the corresponding radius:

$$\beta_{2ex,f} = \beta_{2ds,f} - \tau = \beta_{2ds,f} - \varepsilon \cdot \Delta\beta_f \quad . \tag{12}$$

Only the main results are be presented here. A detailed analysis will be prepared by the author for a further publication. With respect to the total pressure increase $\Delta p_t$ the design

|  | $\Delta p_t$ | $\eta_{ts}$ | $\mu_{3D}$ | $\mu_{q3D}$ |
|---|---|---|---|---|
| Design goal | 1500 Pa | 36.8 % | | |
| Without angle corr. | 880 Pa | 6.6 % | 0.680 | 0.736 |
| With angle corr. | 1242 Pa | 24.2 % | 0.737 | 0.785 |
| Schiller angle exagg. | 1539 Pa | 30.7 % | 0.765 | 0.818 |
| Fixed angle exagg. | 1500 Pa | 30.7 % | 0.764 | 0.811 |
| Weighted angle exagg. | 1537 Pa | 30.9 % | 0.786 | 0.815 |

**TABLE 4**. CHARACTERISTIC VALUES AT THE DESIGN POINT

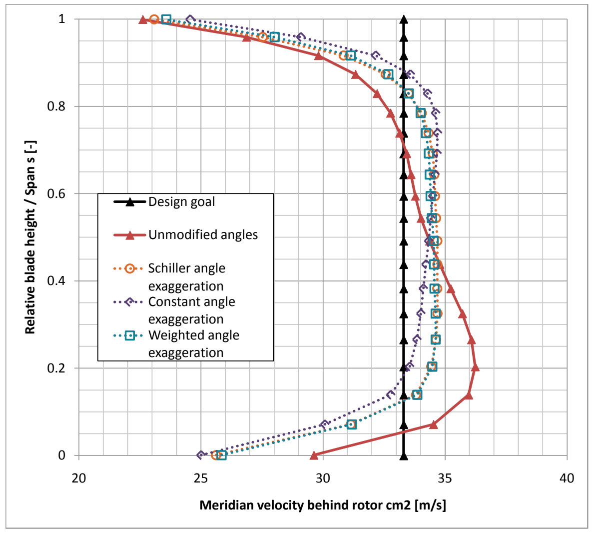


**FIGURE 29**. MERIDIAN VELOCITY DISTRIBUTION BEHIND THE ROTOR – COMPARISON OF ANGLE EXAGGERATION METHODS

point was found to be reached applying the angle exaggeration method suggested by Schiller [10]. Concerning the *constant angle exaggeration* method, a value of $\tau = 3^\circ$ was adequate and for the *weighted angle exaggeration* method the optimum parameter was $\varepsilon = 0.30$. An overview of the results can be found in tab. 4.

It is remarkable that both angle correction and exaggeration methods lead to increased slip factors. Apart from a slight offset between the quasi-3D and the 3D predictions of the slip factor this tendency can already be observed on the basis of the quasi-3D calculations. Without trailing edge profile angle modifications the design goal can not at all be reached. Applying an angle correction improves the situation but only by angle exaggeration it is possible to reach the design goal. While the characteristic values of the fans with an angle exaggeration method applied differ only marginally, some differences can be observed concerning the distribution of the meridian velocity behind the rotor (see fig. 29). All angle exaggeration methods succeed improving the meridian velocity distribution compared to the fan without angle modification (red curve). Both the Schiller and the weighted angle exaggeration method induce a constant meridian velocity distribution whereas the *fixed angle exaggeration* method leads to a slightly tilted curve. Defects can be found for all curves in the area of the hub and the shroud which is due to the wall friction.

Fig. 30 depicts the principles of the angle correction and exaggeration methods. The distribution of the fan with unmodified angles is tilted – the total pressure increase at the hub is far higher than at the shroud (red curve). As a consequence of the angle correction the curve is rendered upright (green curve) and the angle exaggeration moves the distribution towards higher values of $\Delta p_t$. While the *constant angle exaggeration* method alters the slope of the distribution, the other two methods lead to nearly identical curves that almost have the same shape as the ones given by means of the angle correction method.

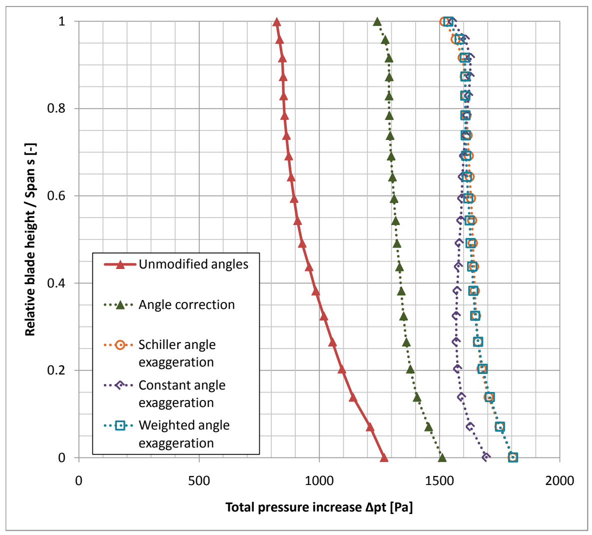


**FIGURE 30**. TOTAL PRESSURE INCREASE DISTRIBUTION – COMPARISON OF ANGLE EXAGGERATION METHODS

## CONCLUSION AND OUTLOOK

As presented, the predictions that can be made using the plane potential theory might differ substantially from the ones given by the one dimensional theory. It could be shown that for instance the prediction of the deviation between trailing edge blade angles and the flow angles behind the rotor can be made with good accuracy. In contrast to slip factors given in the literature, e.g. by Pfleiderer [2], the presented method is able to calculate a slip factor modelling a large variety of influences without relying on empirical data. This includes characteristics such as the exact profile shape, inlet flow conditions, staggering and the number of blades.

It was shown that by means of the presented quasi-3D method predictions can be made not only for single cascade sections but for the entire impeller. These predictions have a considerably higher precision than those made by the 1D mean line theory. Tendencies that were identified by the quasi-3D method, e.g. concerning the slip factor, total pressure distributions or the influence of parameters like the blade thickness, could be confirmed with 3D CFD computations.

It was also shown that the method can readily be used to examine and evaluate angle correction and exaggeration methods. It is therefore highly feasible to be used in an integrated design and optimisation process which is suggested by the authors [21]. Due to the low computational effort the method is capable of significantly reducing the number of time- and resource-consuming CFD simulations in iterative design processes. To give one example: A 3D CFD calculation as described in the previous sections requires about 2 hours of time to converge properly using a single CPU on up-to-date standard PC hardware. A 2D potential flow calculation, on the other hand, requires only about one second on the same system. If a full impeller is modelled using 20 2D sections, a number of 360 impellers can be evaluated in the same amount of time that is necessary to perform one single 3D CFD calculation. While, of course, the cost of CFD simulations is constantly diminishing, the described method can contribute to an efficient utilisation of available resources. It might as well be used for interactive blade section design as the results are available practically in real-time.

As mentioned, the dependency of the meridian velocity from the vortex distribution at design and offdesign conditions is currently prepared for publication by the authors [21]. It will be integrated into the current method and presented in a further publication. Furthermore, the combined analysis of rotor and guiding vanes and a simplified calculation of the boundary layer are possible extensions to the method which are being considered by the authors.

## NOMENCLATURE

**Latin symbols**

| | |
|---|---|
| $b$ | Balancing factor |
| $c$ | Absolute velocity, chord length |
| $C_p$ | Pressure coefficient |
| $d$ | Diameter |
| $e$ | Axial component of the blade length |
| $f$ | Maximum camber |
| $g$ | Position of the maximum camber |
| $i$ | Inlet flow incidence angle $i = \beta_{1,f} - \beta_{1,p}$ |
| $l$ | Length |
| $m$ | Hub to tip ratio |
| $o$ | Offset |
| $p$ | Pitch, pressure |
| $p/c$ | Pitch to chord ratio |
| $r$ | Radius |
| $Re$ | Reynolds number |
| $s$ | Relative blade height/span |
| $t$ | Blade thickness |
| $T$ | Temperature |
| $u$ | Circumferential velocity |
| $\dot{V}$ | Volumetric flow |
| $w$ | Relative velocity |
| $z$ | Number of blades |

**Greek Symbols**

| | |
|---|---|
| $\beta_{1,f}$ | Cascade inlet flow angle |
| $\beta_{1,p}$ | Cascade leading edge camber line/profile angle |
| $\beta_{2,f}$ | Cascade outlet flow angle |
| $\beta_{2,p}$ | Cascade trailing edge camber line/profile angle |
| $\Delta\beta$ | Blade turning angle $\Delta\beta = \beta_{1,p} - \beta_{2,p}$ |
| $\chi$ | Pfleiderer coefficient |
| $\delta$ | Outlet flow deviation angle $\delta = \beta_{2,f} - \beta_{2,p}$ |
| $\delta$ | Specific diameter |
| $\varepsilon$ | Angle exaggeration factor |
| $\gamma_1$ | Profile leading edge camber line/profile angle |
| $\gamma_2$ | Profile trailing edge camber line/profile angle |
| $\eta$ | Efficiency |
| $\lambda$ | Stagger angle |
| $\mu$ | Slip factor |
| $\rho$ | Density |
| $\sigma$ | Specific speed |
| $\tau$ | Exaggeration angle |

**Abbreviations, subscripts and superscripts**

| | |
|---|---|
| 1 | Impeller inlet |
| 2 | Impeller outlet |
| a | Ambient |
| CFD | Computational fluid dynamics |
| ds | Design |
| ex | Exaggerated |
| f | Related to the flow |
| FS | Free slip boundary condition (wall friction disabled) |
| LE | Leading edge |
| ML | Mean line theory |
| NS | No slip boundary condition (wall friction enabled) |
| p | Related to the profile |
| PF | Potential flow |
| Pfl | Pfleiderer |
| q3D | Quasi three dimensional |
| t | Total |
| TE | Trailing edge |
| ts | Total to static |

## REFERENCES


[1] Bohl, W., and Elmendorf, W., 2008. *Strömungsmaschinen 1*, $10^{th}$ ed. Vogel Verlag, Wuerzburg, Germany.

[2] Pfleiderer, C., and Petermann, H., 2005. *Strömungsmaschinen*, $7^{th}$ ed. Springer Verlag, Berlin, Germany.

[3] Dixon, S., and Hall, C., 2010. *Fluid Mechanics and Thermodynamics of Turbomachinery*, $6^{st}$ ed. Butterworth-Heinemann.

[4] Lakshminarayana, B., 1996. *Fluid Dynamics and Heat Transfer of Turbomachinery*, $1^{st}$ ed. John Wiley & Sons, New York City, USA.

[5] Eck, B., 1973. *Fans*, $1^{st}$ ed. Pergamon Press.

[6] Hetzer, T., 2010. "Exact solution of the plane flow and slip factor in arbitrary radial blade channels and extended design method for radial impellers". In Proceedings of the ASME 2010 International Mechanical Engineering Congress & Exposition. Paper number IMECE2010-39081.

[7] Qiu, X., Japikse, D., Zhao, J., and Anderson, M., 2010. "Analysis and validation of a unified slip factor model for impellers at design and off-design conditions". In Proceedings of the ASME Turbo Expo 2010: Power for Land, Sea and Air GT2010. Paper number GT2010-22164.

[8] Lieblein, S., 1959. Incidence and deviation angle correlations for compressor cascades. Technical report NASA-TM-X-56232, NASA Lewis Research Center, Cleveland (Ohio), USA.

[9] Brodersen, S., 1987. "Experimentelle Untersuchungen an hochbelasteten Axialventilatoren mit kleinem Nabenverhltnis". PhD Thesis, Technical University, Braunschweig, Germany.

[10] Schiller, F., 1984. "Theoretische und experimentelle Untersuchungen zur Bestimmung der Belastungsgrenze bei hochbelasteten Axialventilatoren". PhD Thesis, Technical University, Braunschweig, Germany.

[11] Smith, H., 2010. "Erweiterung eindimensionaler Auslegungsverfahren fr axiale Schaufelgitter durch exakte Berechnung der zweidimensionalen reibungsfreien Strmung". Diploma Thesis, University, Erlangen, Germany.

[12] Kümmel, W., 2007. *Technische Strömungsmechanik – Theorie und Praxis*, $3^{rd}$ ed. Teubner Verlag.

[13] Bohl, W., 2005. *Strömungsmaschinen 2*, $7^{th}$ ed. Vogel Verlag, Wuerzburg, Germany.

[14] Riegels, F., 1958. *Aerodynamische Profile*, $1^{st}$ ed. Oldenbourg Verlag, Muenchen, Germany.

[15] Paraschivoiu, I., 2003. *Subsonic Aerodynamics*, $1^{st}$ ed. Presses Internationales Polytechnique.

[16] Lewis, R., 1996. *Turbomachinery Performance Analysis*, $1^{st}$ ed. John Wiley & Sons, New York City, USA.

[17] Katz, J., and Plotkin, A., 1991. *Low Speed Aerodynamics – From Wing Theory to Panel Methods*, $1^{st}$ ed. McGraw-Hill, New York City, USA.

[18] Martensen, E., 1959. "Berechnung der Druckverteilung an Gitterprofilen in ebener Potentialströmung mit einer Fredholmschen Integralgleichung". *Archive for Rational Mechanics and Analysis,* ***3***(1).

[19] Menter, F., 1993. "Zonal two equation $k-\omega$ turbulence models for aerodynamic flows". In AIAA $24^{th}$ Fluid Dynamics Conference. Paper number AIAA-93-2906.

[20] Cebeci, T., Shao, J., Kafyeke, F., and Laurendeau, E., 2005. *Computational Fluid Dynamics for Engineers*, $1^{st}$ ed. Springer-Verlag.

[21] Semel, M., Epple, P., Miclea, M., Delgado, A., and Smith, H., 2011. "Extended meanline theory for axial fans – analytic calculation of the flow characteristics for off-design points". In Proceedings of the ASME Turbo Expo – Turbine Technical Conference & Exposition ASME TE 2011. Submitted paper, number GT2011-46268.

[22] Carolus, T., 2009. *Ventilatoren - Aerodynamischer Entwurf, Schallvorhersage, Konstruktion*, $2^{nd}$ ed. Vieweg+Teubner Verlag, Wiesbaden, Germany.

[23] Schlichting, H., and Gersten, K., 2006. *Grenzschicht-Theorie*, $10^{th}$ ed. Springer Verlag.

[24] Epple, P., 2009. "Modern Design and Applications to Radial Fans". PhD Thesis, University, Erlangen, Germany.

[25] Bommes, L., Fricke, J., and Grundmann, R., eds., 2002. *Ventilatoren*, $2^{nd}$ ed. Vulkan Verlag, Essen, Germany.